The AAPS Journal (2019) 21: 16
DOI: 10.1208/s12248-018-0284-8

Research Article

Survival Prolongation Index as a Novel Metric to Assess Anti-Tumor Activity in Xenograft Models

Fiona Chandra,[1,3] Lihi Zaks,[2] and Andy Zhu[1]

Received 27 July 2018; accepted 11 December 2018; published online 9 January 2019

Abstract. A single efficacy metric quantifying anti-tumor activity in xenograft models is useful in evaluating different tumors' drug sensitivity and dose-response of an anti-tumor agent. Commonly used metrics include the ratio of tumor volume in treated *vs*. control mice (T/C), tumor growth inhibition (TGI), ratio of area under the curve (AUC), and growth rate inhibition (GRI). However, these metrics have some limitations. In particular, for biologics with long half-lives, tumor volume (TV) of treated xenografts displays a delay in volume reduction (and in some cases, complete regression) followed by a growth rebound. These observed data cannot be described by exponential functions, which is the underlying assumption of TGI and GRI, and the fit depends on how long the tumor volumes are monitored. On the other hand, T/C and TGI only utilizes information from one chosen time point. Here, we propose a new metric called Survival Prolongation Index (SPI), calculated as the time for drug-treated TV to reach a certain size (e.g., 600 mm^3) divided by the time for control TV to reach 600mm^3 and therefore not dependent on the chosen final time point t_f. Simulations were conducted under different scenarios (i.e., exponential *vs*. saturable growth, linear *vs*. nonlinear kill function). For all cases, SPI is the most linear and growth-rate independent metric. Subsequently, a literature analysis was conducted using 11 drugs to evaluate the correlation between pre-clinically obtained SPI and clinical overall response. This retrospective analysis of approved drugs suggests that a predicted SPI of 2 is necessary for clinical response.

KEY WORDS: antitumor activity; tumor growth inhibition; xenograft.

INTRODUCTION

The most commonly used *in vivo* pre-clinical model in oncology is the mouse xenograft model which involves subcutaneous implantation of a human cell line/tumor into an immune-compromised host mouse (1). The xenograft model represents an oversimplification of human cancer, as it does not account for the complexities of tumor metastasis, host immunity, tumor heterogeneity, and the development of resistance that is routinely observed in cancer patients. Nevertheless, the drug exposure-response relationships derived from these models is still useful for understanding the degree of anti-tumor activity associated with an investigational drug and allows in vivo interpretation of tumor growth inhibition data to inform early clinical development decisions. More recently, the advances in immunotherapies have led to the development of patient-derived xenograft models in chimeric mice transplanted with human immune system (2). The diversity of these xenograft models in multiple cancer types coupled with next-generation sequencing tools also have the potential to inform personalized medicine (3).

Mathematical modeling is often used to translate efficacy in xenograft models to the clinical setting by fitting the efficacy data to a dynamic model. While these dynamic models provide a better understanding of predicted clinical responses (4–6), a single metric quantifying anti-tumor response in animal is useful in the discovery and selection of potential anticancer drugs. The metric can be used to evaluate drug sensitivity and dose-response of a therapeutic agent and is still used to predict clinical activity (1). Traditionally, an exposure-based approach is used where the drug exposure which leads to tumor stasis is selected as the predicted clinical efficacious exposure (7). However, it is unclear whether stasis in xenograft models translate to clinical response. In this paper, we analyze the correlation of various

Electronic supplementary material The online version of this article (https://doi.org/10.1208/s12248-018-0284-8) contains supplementary material, which is available to authorized users.

[1] Translation Modeling and Simulation, DMPK, Takeda Pharmaceuticals, 35 Landsdowne St, Cambridge, Massachusetts 02139, USA.
[2] Department of Bioengineering, University of Pennsylvania, Philadelphia, Pennsylvania, USA.
[3] To whom correspondence should be addressed. (e–mail: fiona.a.chandra@gmail.com)

1550-7416/18/0200-0001/0 © 2018 American Association of Pharmaceutical Scientists

metrics with clinical responses. Current metrics commonly used in the literature include tumor growth inhibition (TGI), the ratio of tumor volume in the treated *vs*. control mice (T/C), and growth rate inhibition (GRI) (8–11). Both T/C and TGI are calculated by looking at only the initial and final tumor volumes between the control and treated tumor without taking into account the dynamics in between. Another method to compare treated tumor volume data is using the ratio of the area under the curve (AUC) of the treated and control tumor volume data. In addition to these metrics, GRI is often used in analyzing tumor xenograft data. In calculating GRI, tumor growth curves are fitted to an exponential function to obtain the apparent growth rates of the treated and control tumor (4). The mathematical definitions of these metrics are given in the "Methods" section.

The limitations of TGI and the benefits of the rate-based metric similar to GRI was discussed by Hather *et al.* (11). These benefits include the requirement for lower number of animals and less dependence on the final time point for data that fits exponential functions. However, for biologics which have longer half-lives than small molecule drugs, the tumor growth curve for treated xenograft models displays both a delay in tumor volume reduction and in some cases also a complete regression followed by a delayed regrowth (Fig. 1). These curves cannot be described by an exponential function. In addition, when comparing efficacy of drugs in different xenograft studies, the time of last measurement of these studies may differ, resulting in different fitted growth rate. For uniformity, the data is often truncated to a fixed time point (e.g., 21 days) but this could obscure the true difference in potency of different drugs or different doses which may become apparent in later time points. In addition, different tumor growth rates may call for different optimal truncation time point, with data from slow growing tumors requiring longer observation time to distinguish drug effects.

In this paper, we introduce a new metric called the Survival Prolongation Index (SPI), which is calculated using the times at which the control and treated tumor grow to a threshold volume. This metric bypasses the issue of truncating the data to choose the same "final time point" across studies. To evaluate the performance of TGI, AUC, GRI, and SPI, we compare the correlation of drug kill rates with each metric using simulated data from a dynamic model. Identifying kill rates of drugs, or at least their relative kill rates, is important in selecting candidate drugs and establishing correlations with different drug or target properties.

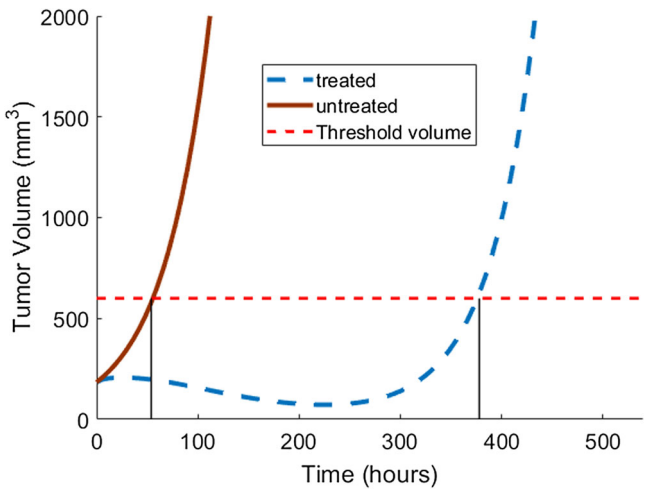

Fig. 1. Simulation of a typical mouse xenograft tumor volume profile after treatment with a biologic. The simulation was generated using the exponential growth rate and linear kill function model (defined as scenario 1 in the manuscript). The red line is the untreated control tumor volume and the blue dashed line is the treated tumor volume. Vertical lines mark the time for control and treated tumor to reach the threshold volume

In general, tumor volume in response to drug treatment can be accurately captured by dynamic ODE systems with exponential growth and transit compartment. The most widely used model is the semi-mechanistic model proposed by Simeoni *et al.* (5). In the original model, tumor growth switches from exponential to linear beyond a threshold tumor mass; however, the model can and has been adapted to a simple exponential growth model depending on the data (12). We evaluated the four metrics for data simulated using different types of growth and kill rates. Wong *et al.* has shown that predicted TGI correlates with clinical response rate well (13). We thus evaluated the performance of these metrics for real drugs by correlating the predicted metric in human to clinical response rates of drugs with available clinical data, including those analyzed in (13).

METHODS

TV data can be summarized using various metrics. TGI is calculated as the difference in final tumor volume of treated *vs*. control divided by the difference of the final and initial control tumor volume.

$$\mathrm{TGI} = \frac{\mathrm{TV}_{\mathrm{control}}(t_{\mathrm{final}}) - \mathrm{TV}_{\mathrm{treated}}(t_{\mathrm{final}})}{\mathrm{TV}_{\mathrm{control}}(t_{\mathrm{final}}) - \mathrm{TV}_{\mathrm{control}}(0)} \tag{1.1}$$

The normalized AUC method is calculated as the difference in area under the tumor growth curve between control and treated tumor, normalized by the area under the curve for the control tumor.

$$\mathrm{AUC} = \frac{\mathrm{AUC}_{\mathrm{control}} - \mathrm{AUC}_{\mathrm{treated}}}{\mathrm{AUC}_{\mathrm{control}}} \tag{1.2}$$

In the GRI calculation, tumor volume data is fitted to an exponential function. GRI is then calculated as:

$$\mathrm{GRI} = \frac{\mathrm{gr}_{\mathrm{control}} - \mathrm{gr}_{\mathrm{treated}}}{\mathrm{gr}_{\mathrm{control}}} \tag{1.3}$$

where $\mathrm{gr}_{\mathrm{control}}$ is the fitted exponential growth rate of the control tumor and $\mathrm{gr}_{\mathrm{treated}}$ is the growth rate of the treated group. For most of the analysis presented in this paper, both TGI and GRI are calculated with 60 days as the final timepoint unless noted otherwise.

The Survival Prolongation Index (SPI) is calculated as the time for the treated tumor volume to reach a certain size divided by the time for the control tumor to reach the same size.

$$\mathrm{SPI} = \frac{\mathrm{time}(\mathrm{TV}_{\mathrm{treated}} = \mathrm{TV}_{\mathrm{threshold}})}{\mathrm{time}(\mathrm{TV}_{\mathrm{control}} = \mathrm{TV}_{\mathrm{threshold}})} \tag{1.4}$$

This is similar to the tumor efficacy index (TEI) proposed previously and can be intuitively understood as the prolongation of survival (5). SPI of 2 means that it takes the treated tumor twice as long to reach the threshold volume as it takes the untreated tumor to reach the same volume. In this paper, we use 600 mm^3 as the threshold volume $\mathrm{TV}_{\mathrm{threshold}}$, the rationale for which is further discussed in the "Results" section.

Simulations of Hypothetical Tumor Growth Data

Drug pharmacokinetics was simulated using a two-compartment linear model with parameters similar to those reported for antibodies (see SI Table S1 for parameter values). Tumor volume after a treatment was simulated using Simeoni model with four transit compartments (5). The growth and kill functions are varied in order to obtain the correlation between the "real" kill rate and efficacy metric.

$$\begin{aligned}
&\mathrm{TV}_{\mathrm{tot}} = \mathrm{TV1} + \mathrm{TV2} + \mathrm{TV3} + \mathrm{TV4}\\
&\frac{\partial \mathrm{TV1}}{\partial t} = f_{\mathrm{grow}}(\mathrm{TV1}) - f_{\mathrm{kill}}(C, \mathrm{TV1})\\
&\frac{\partial \mathrm{TV2}}{\partial t} = f_{\mathrm{kill}}(C, \mathrm{TV1}) - \tau \mathrm{TV2}\\
&\frac{\partial \mathrm{TV3}}{\partial t} = \tau \mathrm{TV2} - \tau \mathrm{TV3}\\
&\frac{\partial \mathrm{TV4}}{\partial t} = \tau \mathrm{TV3} - \tau \mathrm{TV4}\\
&\mathrm{TV1}(0) = 183\mathrm{mm}^3, \mathrm{TV2}(0) = \mathrm{TV3}(0) = \mathrm{TV4}(0) = 0
\end{aligned} \tag{1.5}$$

where C is the drug concentration in the plasma, $\mathrm{TV}_{\mathrm{tot}}$ is the total tumor volume, TV1-TV4 are the tumor volumes in each transit compartment and τ is the transit delay parameter. f_{grow} and f_{kill} are the growth and kill functions, which vary in the different scenarios tested and defined below.

We compared TGI, GRI, and SPI for simulated tumor volume with exponential and saturable growth rate as well as linear or nonlinear kill function. The exponential growth function and linear kill function are defined as:

$$f_{\mathrm{grow}}(\mathrm{TV1}) = k_{\mathrm{grow}} \mathrm{TV1} \tag{1.6}$$

$$f_{\mathrm{kill}}(C, \mathrm{TV1}) = k_{\mathrm{kill}} C \cdot \mathrm{TV1} \tag{1.7}$$

where k_{grow} is the growth rate of the tumor and k_{kill} is the kill rate of the drug acting on the tumor. In the early phase of tumor growth, tumor growth follows an exponential growth rate. However, as the tumor becomes bigger, the growth rate slows down, becomes linear, and then plateaus due to space and nutrient restriction. This behavior is well described by a saturable growth function described in (5) and shown below:

$$f_{\mathrm{grow}}(\mathrm{TV1}) = \frac{L0 \cdot \mathrm{TV1}}{\left(1 + \left(\frac{L0}{L1}\mathrm{TV1}\right)^{\psi}\right)^{\frac{1}{\psi}}} \tag{1.8}$$

where $L0$ is the parameter characterizing the exponential growth phase and $L1$ characterizes the linear growth phase. The parameter ψ describes the transition between the exponential and linear phases.

And the nonlinear kill function takes the form of:

$$f_{\mathrm{kill}}(C, \mathrm{TV1}) = \frac{k_{\max} C \cdot \mathrm{TV1}}{K_D + C} \tag{1.9}$$

where $k_{\max}$ is the maximal kill rate of the drug acting on the tumor and K_D is the concentration of the drug where the rate of the tumor kill is half of $k_{\max}$. There were four different scenarios tested: (1) exponential growth and linear kill function, (2) saturable growth and linear kill rate, (3) exponential growth and nonlinear kill function, and (4) saturable growth and nonlinear kill function.

Simulation of Clinical Responses

We compare the correlation of the three metrics to clinical responses for the set of ten anticancer agents presented in (13). In addition, we calculated each metric for approved antibody drug conjugates T-DM1 (Kadcyla) for a total of 11 anti-cancer drugs.

We simulated the predicted tumor volume in human for 11 combinations of anticancer agents and target indications and calculated the predicted AUC, TGI, GRI, and SPI. To do so, we fitted mouse tumor xenograft data using mouse pharmacokinetic parameters. Using the fitted pharmacodynamics parameters and human clinical PK parameters obtained from the literature, we simulated predicted tumor volume in human after 21 days of treatment using clinical dosing regimen. We then calculated the AUC, TGI, GRI, and SPI of the predicted tumor volume and correlated each metric to the clinical response rate, similar to the analysis presented in (13). We chose 21 days as the final time point of AUC, TGI, and GRI measurements to match the calculated TGI in (13).

The preclinical efficacy data were obtained from (13,14). Clinical response rates for T-DM1 was obtained from (14). One of the limitations of this kind of analysis is the heterogenicity of the data. While Wong *et al.* performed their own preclinical PK and xenograft studies, we obtain mouse PK parameters or data of the same ten drugs from the literature and xenograft data from (13). Slight differences in PK can propagate to the estimated PD parameters, thus resulting in different simulated tumor volume profiles. References for preclinical and clinical PK data are shown in Table I (6,12,15–30). Xenograft data for T-DM1 was obtained from (12).

RESULTS

Correlation Between Efficacy Metrics and Kill Rates

Scenario 1: Exponential Growth and Linear Kill Function

In the first scenario, we assume that the tumor is growing exponentially (Eq. 1.6) and the kill rate of the drug is linear with the plasma concentration (Eq. 1.7). As illustrated in Fig. 2a, b, both AUC ratio and TGI are easily

Table I. Predicted Metrics for 11 Drug/Target Indications and Their Clinical Response Rates

Drug	Predicted SPI (unitless)	Predicted TGI (%)	Predicted AUC (unitless)	Predicted GRI (%)	Clinical response (%)	Clinical PK refs	Preclinical PK refs
Erlonitib	3.8	96.9	.85	86.3	71	(21)	(20)
Trastuzumab	2.1	79.4	.42	64.3	15	(23)	(22)
Sunitinib (renal)	2.6	73.6	.49	52.2	47	(25)	(24)
Sunitinib (colorectal)	1.2	22.5	.08	12.3	1.2	(25)	(24)
Docetaxel	2.6	79.3	.64	56.3	33	(17)	(27)
Dasatinib	5.2	103.5	.85	144.8	90%	(18)	(28)
5-FU	2.7	97.5	.77	101.9	10.3	(16)	(30)
Carboplatin	3.4	110.9	.82	176.9	31	(26)	(15)
Vismodegib (medulloblastoma)	8.9	103.5	.94	176.9	55	(19)	(29)
Vismodegib (colorectal)	1.7	43.4	.25	26.7	0	(19)	(29)
T-DM1	8.4	136.3	.61	136.3	59.7	(12)	(6)

saturated for compounds with high kill rates and do not have the dynamic range to distinguish the potency between these compounds. In other words, all drugs with $k_{kill} > 0.002$ hr^{-1} L/mg would have the same AUC ratio or TGI. GRI is shown to be dependent on the growth rate, and the dynamic range also varies with the growth rate (Fig. 2c). On the other hand, SPI is shown to be completely linear with k_{kill} and has the same slope regardless of the tumor growth rate k_{grow} (Fig. 2d). SPI is also independent of the transit delay parameter τ (see Supplementary Information Fig. S1).

Scenario 2: Saturable Growth and Linear Kill Function

For the saturable growth model (Eq. 1.8), we vary the growth rate by varying the first order growth rate parameter $L0$ and found that all four metrics are dependent on $L0$. However, despite losing the growth rate independence for the saturable growth scenario, SPI still results in the biggest dynamic range with respect to potency k_{kill}. GRI (Fig. 3c) has a wider dynamic range than TGI (Fig. 3a) and AUC (Fig. 3b). For each $L0$

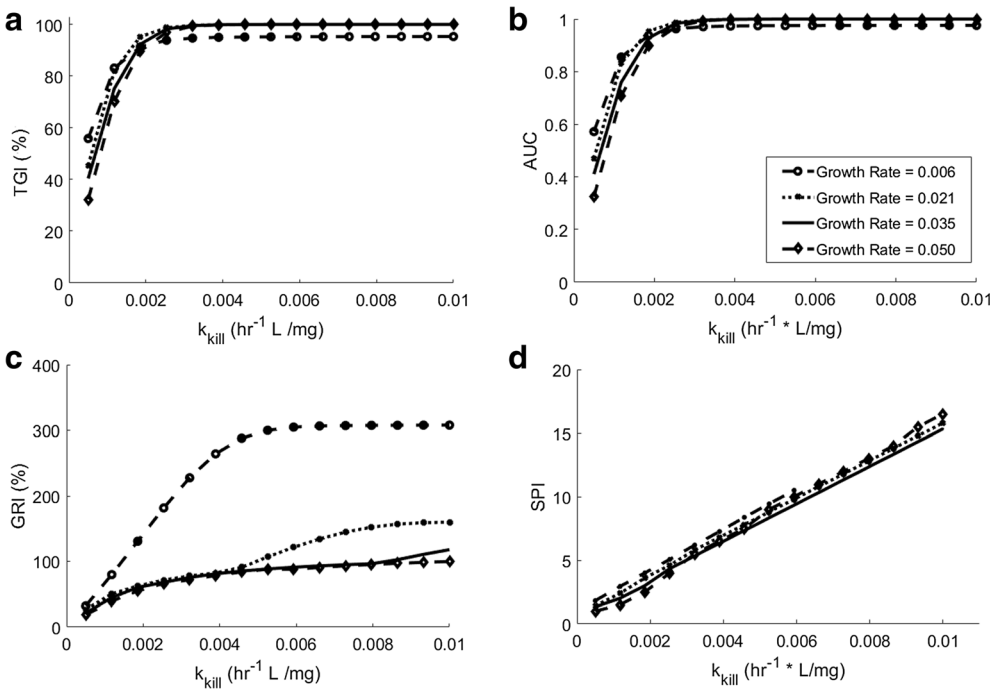

Fig. 2. Relationships between linear kill rate (k_{kill}) with TGI, AUC, GRI, and SPI with increasing tumor growth rate for scenario 1 (exponential growth and linear kill function). SPI is completely linear and growth rate-independent in this scenario. SPI and AUC metrics are dimensionless

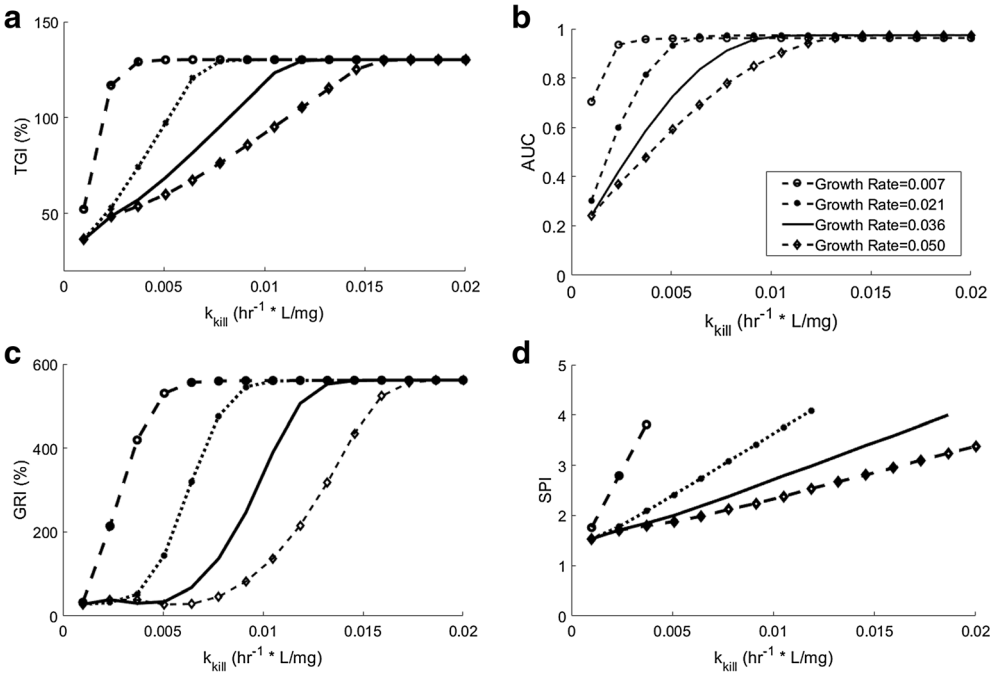

Fig. 3. Relationships between linear kill rate (k_{kill}) with TGI, AUC, GRI, and SPI with increasing tumor growth rate for scenario 2 (saturable growth and linear kill function). All three metrics are dependent on the tumor growth rate in this scenario, but SPI remains linear. SPI and AUC metrics are dimensionless

value, SPI is again completely linear with k_{kill}; however, the slope changes depending on the $L0$ (Fig. 3d). The slope also changes incrementally with transit delay parameter τ (data not shown).

Scenario 3: Exponential Growth and Nonlinear Kill Function

In the third scenario, we examine the effects of a nonlinear kill function. To separate the effects that stem from nonlinear growth rate with the nonlinear kill function, we revert back to the exponential growth rate (Eq. 1.6) and change the kill function to be nonlinear (Eq. 1.). For this nonlinear function, there are two parameters that affect the overall potency of the drug: $k_{\max}$ and K_D. The effect of $k_{\max}$ is similar to the linear parameter k_{kill}, so we focus our analysis on the effect of K_D, the parameter representing the IC50 value or sensitivity of the drug. We vary K_D while keeping k_{max} constant. All four metrics (AUC, TGI, GRI, and SPI) are nonlinear with K_D; however, AUC and SPI are most independent of tumor growth rate (Fig. 4).

Scenario 4: Saturable Growth and Nonlinear Kill Function

In the final scenario, we combine the effects of saturable growth with a nonlinear kill function. As also seen in scenario 3, SPI is nonlinear with K_D due to the nonlinear kill function (Fig. 5d). In scenario 4, SPI is more dependent on the tumor growth rate than in scenario 3 (as the growth rate dependence stems from the nonlinearity of the saturable growth function); however, it is still the most growth rate-independent metric compared to AUC, TGI, or GRI (Fig. 5a–c). For faster growing tumors, SPI also gives a better dynamic range than the other metrics.

SPI and Threshold Tumor Volume

The effect of changing the threshold tumor volume is shown in the SI Fig. S4 for exponentially growing tumor and Fig. S5 for saturable growth. For drugs with linear kill function, SPI remains linear with kill rate for all threshold tumor volumes analyzed, but the slope changes depending on the threshold tumor volume. Within a range of threshold volumes, the slope of SPI *vs*. kill rate remains the same, but the slope switches at certain volumes. The volume at which the slope switches depends on the tumor growth rate, time delay parameter τ, and the drug's half-life which affects the time at which drug concentration becomes low enough to allow for tumor regrowth. While this implies that SPI analyzed using different threshold volumes cannot be compared, SPI values analyzed using the same threshold volume would be linear and consistent across different tumor growth rates.

A consistent trend across these parameters is that a smaller threshold tumor volume leads to a wider dynamic range. However, the threshold tumor volume must remain above the initial increase in tumor volume before treatment shows its effect and thus the threshold should depend on the time delay τ of the drug effect. The threshold volume should also be large enough to account for experimental variability. For most xenograft models, we have found a threshold tumor volume of around 600 mm^3 to be suitable.

SPI and Length of Study

The length of observation time in different xenograft studies tends to vary depending on several factors. To maintain uniformity across studies, the data tends to be truncated at a chosen time point for the TGI or GRI

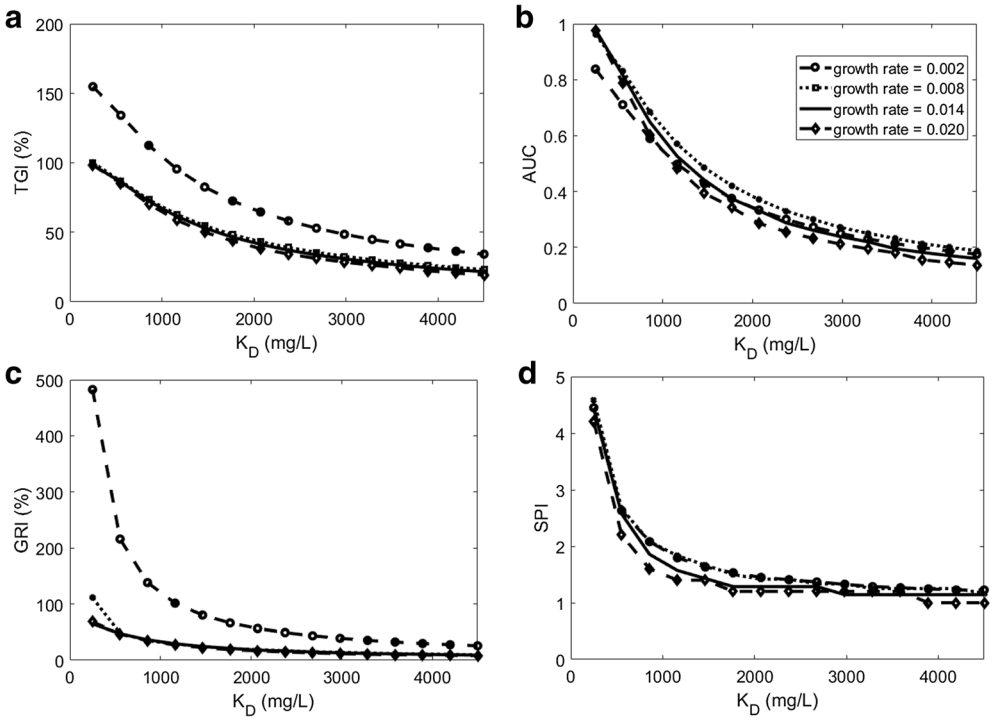

Fig. 4. Relationships between drug sensitivity (K_D) with TGI, AUC, GRI, and SPI with increasing tumor growth rate for scenario 3 (linear growth and nonlinear kill function). SPI is no longer linear with drug sensitivity but remains growth rate-independent. SPI and AUC metrics are dimensionless

calculation; however, in cases where drugs show a delayed response and a temporary regression, TGI and GRI values can change depending on the chosen final time points. Since SPI marks the time the tumor volume reaches a threshold, there is no need to truncate observed tumor volume data for uniformity. For slow- growing tumor models, SPI may require

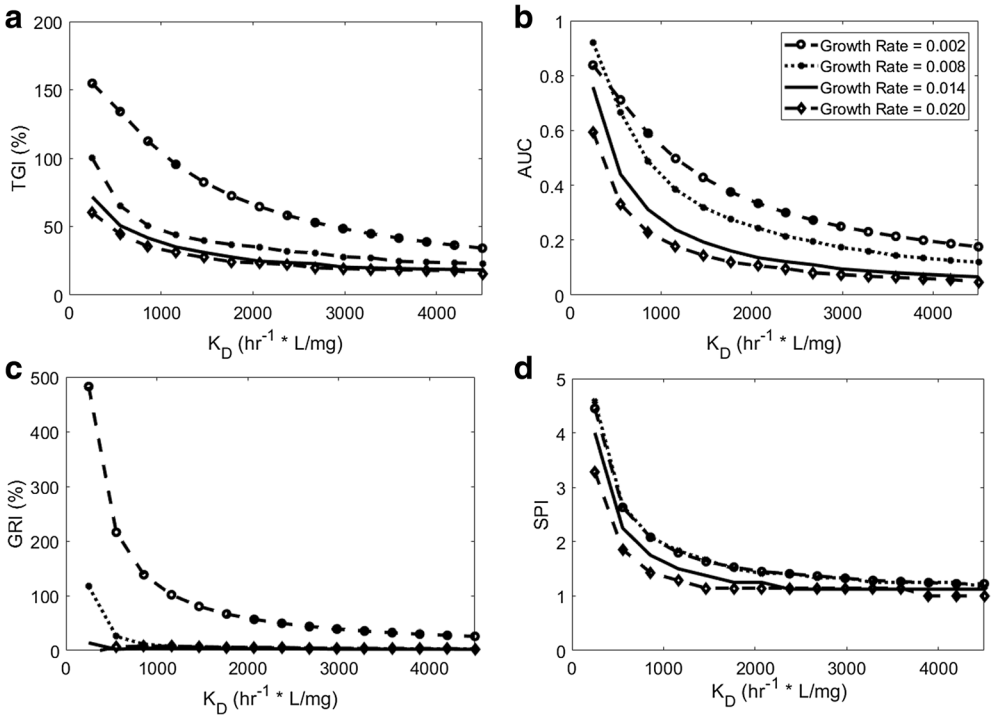

Fig. 5. Relationships between drug sensitivity (K_D) with TGI, AUC, GRI, and SPI with increasing tumor growth rate for scenario 4 (saturable growth and nonlinear kill function). SPI is no longer linear with drug sensitivity but there is growth rate dependency; however, the growth rate dependence is less significant than the other metrics. SPI and AUC metrics are dimensionless

longer observation time to capture the rebound time. However, for faster growing tumor models, such as those typically used to test immuno-oncology drugs, a short observation time will be sufficient.

In real preclinical data, there are cases where the dose given would be too high, resulting in complete regression of the tumor and no rebound within the observed time. In such cases, to calculate the SPI, we take the final observed volume and simulate the tumor growth using the control tumor growth rate. When the final tumor volume data is zero or below the limit of quantification, we simulate the tumor growth from the volume equals to the limit of quantification. When multiple data sets have zero tumor volume, SPI would not be able to distinguish the potency between these data sets, but the same limitation is true for AUC, TGI, and GRI calculations. The incomplete data could obscure the true potency of the drug, thus an appropriately designed dose-ranging xenograft studies that allows for observation of the tumor rebound would be important.

Application to a Dose-Ranging Efficacy Study

One of the utilities of mouse xenografts is a dose-ranging efficacy study to aid in preclinical to clinical translation and human efficacious dose prediction. We simulated a dose-ranging study of four doses in an exponentially growing tumor for a drug with linear kill rate (scenario I) as shown in Fig. 6a. AUC, TGI, GRI, and SPI were analyzed for the resulting simulations. Figure 6a, b shows a rapidly saturating dose response relationship with increasing doses for AUC and TGI. GRI has a wider dynamic range but still shows a saturating effect with increasing dose (Fig. 6c). In contrast, SPI remains linear with dose. Saturating dose-response relationship could confound the translation of preclinical data to clinical efficacious dose.

Correlation with Clinical Response

To determine the relationship between preclinically obtained SPI and clinical response, we looked at ten compounds from the literature (total of 11 drug/target indication combinations). The clinical response rates for the small molecule drugs were taken from (13). As the preclinical PK used to fit the PD parameters here differ than (13), the resulting TGI and clinical response correlation also differs slightly. Individual results are shown in Table I. We fitted the correlation data to a nonlinear sigmoidal function. AUC, TGI, and GRI have similar R^2 values (0.45–0.5, Fig. 7a–c) and SPI shows the best correlation with clinical response (R^2 = 0.74, Fig. 7d). Based on this data set of 11 drugs, SPI of at least 2 is needed to see minimal clinical activity.

DISCUSSION

With the recent surge of biologics as cancer drugs, common metrics for evaluating xenograft efficacy data such as normalized AUC, TGI, and GRI come with certain issues, especially when the doses given to study animals are high enough to temporarily induce complete regression. The potency differences between two drugs or two doses in this case are often only apparent in the rebound phase. For

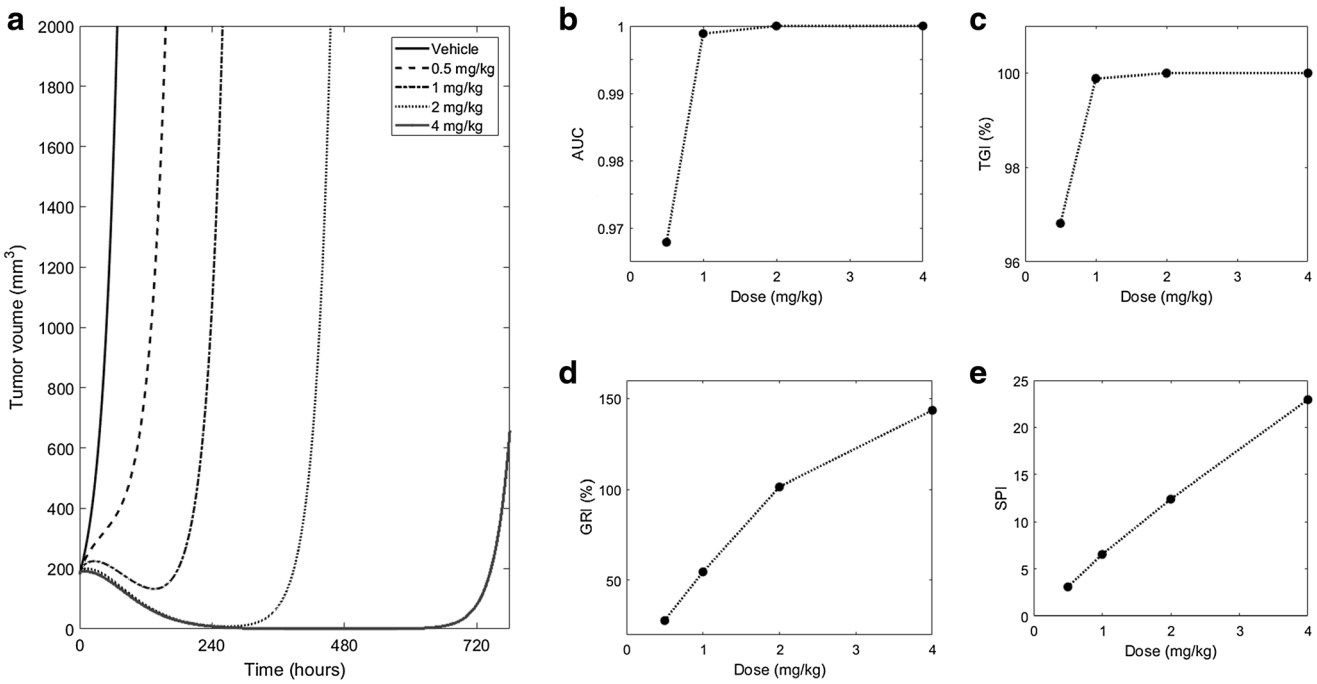

Fig. 6. **a** Simulation of dose-ranging studies in scenario I. Acute doses were simulation for exponentially growing tumor (growth rate = 0.0353 h^{-1}) and linear kill rate (k_{kill} = 0.011 h^{-1} L/mg). **b–c** AUC and TGI evaluated at 21 days rapidly saturate with increasing doses. **d** GRI evaluated at 21 days have a wider dynamic range compared to AUC and TGI but still shows a saturating effect with increasing doses. **e** SPI is linearly correlated with dose

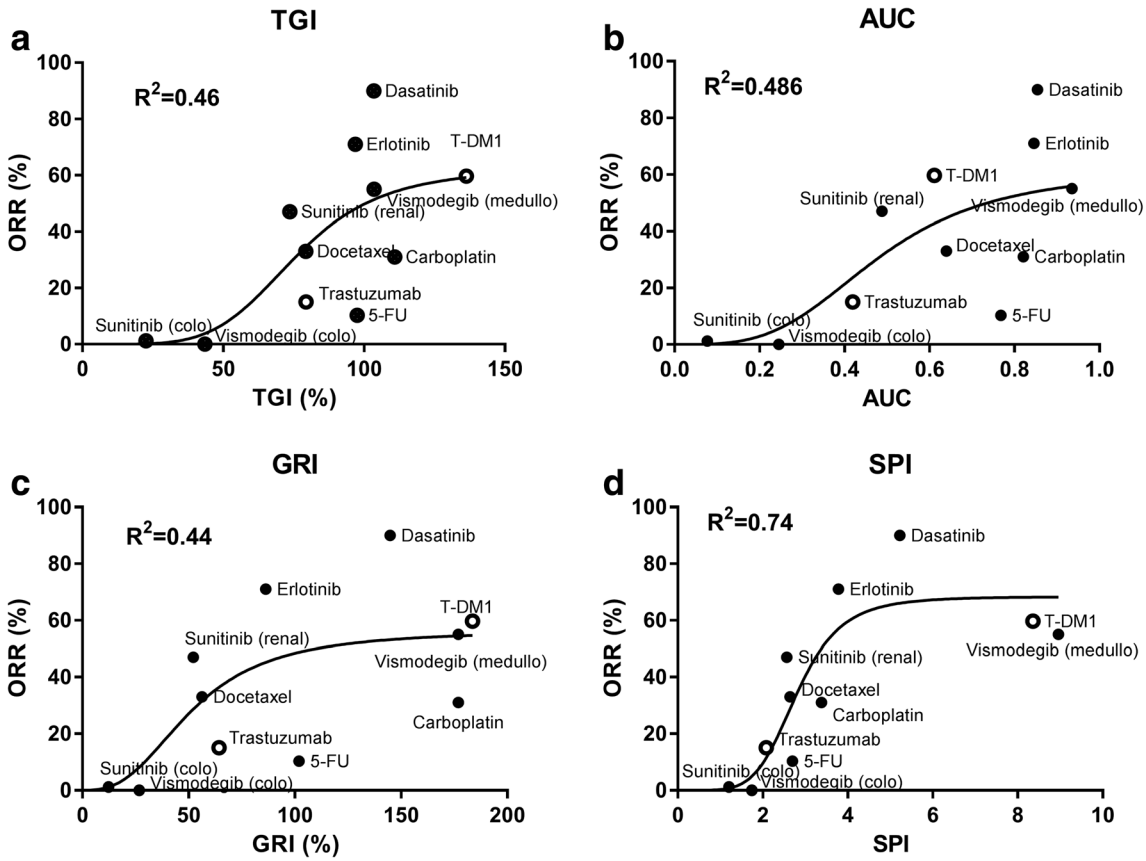

Fig. 7. Correlation between predicted SPI, TGI, and GRI *vs*. clinical overall response rates. AUC, TGI, and GRI show similar correlation with clinical response, while SPI shows the best correlation for this set of data. Open circles (o) denote biologics. SPI and AUC metrics are dimensionless

example, the potency difference between the 1 mg/kg and 3 mg/kg dose of SYD985 in certain tumor models are distinguishable only by the rebound after 30+ days (31). AUC, TGI, and GRI calculations depend on the tumor growth rate, the final observed time point, and response delay and often do not provide a wide enough dynamic range.

When the tumor growth shows saturable behavior, SPI is not growth rate-independent but is still the only metric that linearly correlates with kill rate and thus provides the widest dynamic range. For nonlinear kill functions, SPI is no longer linear with the drug IC50 but is still growth rate-independent. Again, SPI loses some of the growth rate independence when the tumor growth is saturable/non-exponential, but SPI still shows the lowest variation with growth rate compared to AUC, TGI, and GRI.

In our analysis, preclinical PK was obtained from the literature or fitted to literature data; therefore, there is some variability compared to the parameters used by Wong *et al.* The PK differences are one of the factors that contribute to the difference in predicted TGI values between our simulations and Wong *et al.* (13). SPI is better correlated than AUC, TGI, or GRI calculated at 21 days. This may be due to the drugs that show initial high potency followed by a fast rebound, such as in the case for Carboplatin and 5-FU.

SPI bypasses the issue of differing final time points and observation time across studies; however, the use of SPI does warrant a long enough study duration to observe at least the beginning of the rebound phase. An appropriate dose range should be designed to observe rebound within a practical study duration. In addition, with the increasing use of syngeneic tumor models, which tend to grow faster than other tumor models, length of study duration would be less of an issue.

In this paper, we have shown that SPI provides the largest dynamic range with respect to drug potency as well as dose range compared to the other three metrics. In addition, SPI has the best correlation to the clinical overall response rates compared to the other metrics based on 11 anticancer drugs, both small molecules and biologics. Therefore, we propose the use of SPI for preliminary analysis of tumor xenograft data, in particular for biologics and immuno-oncology targets where tumor growth rate may be faster and deeper responses are observed. With its growth rate independence, this kind of metric is also particularly useful for Phase II-like studies where efficacy is compared across a big range of models (32).

Publisher's Note Springer Nature remains neutral with regard to jurisdictional claims in published maps and institutional affiliations.

REFERENCES

1. Voskoglou-Nomikos T, Pater J, Seymour L. Clinical predictive value of the in vitro cell line, human xenograft, and mouse allograft preclinical cancer models. Clin Cancer Res. 2003;9:4227–39.
2. Lai Y, Wei X, Lin S, Qin L, Cheng L, Li P. Current status and perspectives of patient-derived xenograft models in cancer research. J Hematol Oncol. 2017;10:106.
3. Morgan K, Riedlinger G, Rosenfeld J, et al. Patient-derived xenograft models of non-small cell lung cancer and their potential utility in personalized medicine. Front Oncol. 2017;7:2.
4. Zhu A. Quantitative translational modeling to facilitate preclinical to clinical efficacy and toxicity translation in oncology. Future Sci OA. 2018;4:FSO306.
5. Simeoni M, Magni P, Cammia C, de Nicolao G, Croci V, Pesenti E, et al. Predictive pharmacokinetic-pharmacodynamic modeling of tumor growth kinetics in xenograft models after administration of anticancer agents. Cancer Res. 2004;64:1094–101.
6. Singh A, Shah D. Application of a PK-PD modeling and simulation-based strategy for clinical translation of antibody-drug conjugates: a case study with trastuzumab-emtansine (T-DM1). AAPS J. 2017;19:1054–70.
7. Haddish-Berhane N, Shah D, Ma D, et al. On translation of antibody drug conjugates efficacy from mouse experimental tumors to the clinic: a PK/PD approach. J Pharmacokinet Pharmacodyn. 2013;40:557–71.
8. Duan F, Simeone S, Wu R, Grady J, Mandoiu I, Srivastava PK. Area under the curve as a tool to measure kinetics of tumor growth in experimental animals. J Immunol Methods. 2012;382:224–8.
9. Judde J, Rebucci M, Vogt N, et al. Gefitinib and chemotherapy combination studies in five novel human non small cel lung cancer xenografts. Evidence linking EGFT signaling to gefitinib antitumor response. Int J Cancer. 2007;120:1579–90.
10. Wu W, Bi C, Credille KM, Manro JR, Peek VL, Donoho GP, et al. Inhibition of tumor growth and metastasis in non-small cell lung cancer by LY2801651, an inhibitor of several oncokinases, including MET. Clin Cancer Res. 2013;19:5699–710.
11. Hather G, Liu R, Bandi S, et al. Growth rate analysis and efficient experimental design for tumor xenograft studies. Cancer Informat. 2014;13(S4):65–72.
12. Jumbe N, Xin Y, Leipold D, et al. Modeling the efficacy of trastuzumab-DM1, an antibody drug conjugate, in mice. J Pharmacokinet Pharmacodyn. 2010;37:221–42.
13. Wong H, Choo E, Alicke B, et al. Antitumor activity of targeted and cytotoxic agents in murine subcutaneous tumor models correlates with clinical response. Clin Cancer Res. 2012;18:3846–55.
14. Perez E, Barrios C, Eiermann W, et al. Trastuzumab emtansine with or without pertuzumab versus trastuzumab plus taxane for human epidermal growth factor receptor 2-positive, advanced breast cancer: primary results from the phase III MARIANNE study. J Clin Oncol. 2017;35:141–8.
15. Siddik Z, Jones M, Boxall F, Harrap K. Comparative distribution and excretion of carboplatin and cisplatin in mice. Cancer Chemother Pharmacol. 1988;21:19–24.
16. Van Kuilenburg A, Maring J. Evaluation of 5-fluorouracil pharmacokinetic models and therapeutic drug monitoring in cancer patients. Pharmacogenomics. 2013;14:799–811.
17. Slaviero K, Clarke S, McLachlan A, et al. Population pharmacokinetics of weekly docetaxel in patients with advanced cancer. Br J Clin Pharm. 2003;57:44–53.
18. Demetri G, Russo P, MacPherson I, et al. Phase I dose-escalation and pharmacokinetic study of dasatinib in patients with advanced solid tumors. Clin Cancer Res. 2009;15:6232–40.
19. Lu T, Wang B, Gao Y, Dresser M, Graham RA, Jin JY. Semi-mechanism-based population pharmacokinetic modeling of the hedgehog pathway inhibitor vismodegib. CPT Pharmacometrics Syst Pharmacol. 2015;4:680–9.
20. Wu Q, Li M, Li H, Deng CH, Li L, Zhou TY, et al. Pharmacokinetic-pharmacodynamic modeling of the anticancer effect of erlotinib in a human non-small cell lung cancer xenograft mouse model. Acta Pharmacol Sin. 2013;34:1427–36.
21. Lu J, Eppler S, Wolf J, et al. Clinical pharmacokinetics of erlotinib in patients with solid tumors and and exposure-safety relationship in patients with non-small cell lung cancer. Clin Pharmacol Ther. 2006;80:136–45.
22. Hurst S, Ryan A, Ng C. Comparative nonclinical assessments of the proposed biosimilar PF-05280014 and Trastuzumab (Herceptin). BioDrugs. 2014;28:451–9.
23. Quartino A, Hillenbach C, Li J, et al. Population pharmacokinetic and exposure-response analysis for trastuzumab administered using a subcutaneous 'manual syringe' injection or intravenously in women with HER2-positive early breast cancer. Cancer Chemother Pharmacol. 2016;77:77–88.
24. Li J, Ren Y, Yuan Y, Ji SM, Zhou SP, Wang LJ, et al. Preclinical PK/PD model for combined administration of erlotinib and sunitinib in the treatment of A549 human NSCLC xenograft mice. Acta Pharmacol Sin. 2016;37:930–40.
25. Faivre S, Delbaldo C, Vera K, Robert C, Lozahic S, Lassau N, et al. Safety, pharmacokinetic, and antitumor activity of SU11258, a novel oral multitarget tyrosine kinase inhibitor, in patients with cancer. J Clin Oncol. 2006;24:25–35.
26. Van der Vijgh W. Clinical pharmacokinetics of carboplatin. Clin Pharm. 1991;21:242–61.
27. Bradshaw-Pierce E, Eckhardt S, Gustafson D. A physiologically based pharmacokinetic model of docetaxel disposition: from mouse to man. Clin Cancer Res. 2007;13:2768–76.
28. Luo R, Yang Z, Camuso A, et al. Dasatinib (BMS-354825) pharmacokinetics and pharmacodynamic biomarkers in animal models predict optimal clinical exposure. Clin Cancer Res. 2006;12:7180–6.
29. Graham R, Lum B, Cheeti S, et al. Pharmacokinetics of hedgehog pathway inhibitor vismodegib (GDC-0449) in patients with locally advanced or metastatic solid tumors: the role of alpha-1-acid glycoprotein binding. Clin Cancer Res. 2013;17:2512–20.
30. Wattanatorn W, McLeod H, Macklon F, et al. Comparison of 5-fluorouracil pharmacokinetics in whole blood, plasma, and red blood cells in patients with colorectal cancer. Pharmacotherapy. 1997;17:881–6.
31. Van der Lee M, Groothuis P, Ubink R, et al. The preclinical profile of the duocarmycin-based HER2-targeting ADC SYD985 predicts for clinical benefit in low HER2-expressing breast cancers. Mol Cancer Ther. 2015;14:692–703.
32. Gao H, Korn J, Ferretti S, et al. High-throughput screening using patient-derived tumor xenografts to predict clinical trial drug response. Nat Med. 2015;21:1318–25.